Fabrication of bit patterned media using templated two-phase growth

Vignesh Sundar, XiaoMin Yang, Yang Liu, Zhengkun Dai, Bing Zhou, Jingxi Zhu, Kim Lee, Thomas Chang, David Laughlin, and Jian-Gang (Jimmy) Zhu

---

Articles you may be interested in

Antisolvent-assisted powder engineering for controlled growth of hybrid $CH_3NH_3PbI_3$ perovskite thin films
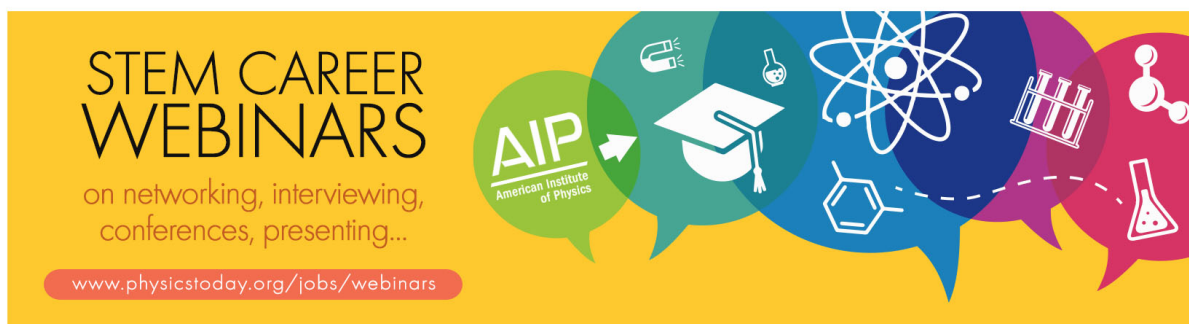APL Materials **5**, 026101 (2017); 10.1063/1.4974942

In situ study of annealing-induced strain relaxation in diamond nanoparticles using Bragg coherent diffraction imaging
APL Materials **5**, 026105 (2017); 10.1063/1.4974865

N-polar InGaN-based LEDs fabricated on sapphire via pulsed sputtering
APL Materials **5**, 026102 (2017); 10.1063/1.4975617

Spin Seebeck effect in insulating epitaxial γ-Fe_2O_3 thin films
APL Materials **5**, 026103 (2017); 10.1063/1.4975618

Interface role in the enhanced photocatalytic activity of TiO_2-$Na_{0.9}Mg_{0.45}Ti_{3.55}O_8$ nanoheterojunction
APL Materials **5**, 026104 (2017); 10.1063/1.4975654

Erratum: "Enhancing polarization by electrode-controlled strain relaxation in $PbTiO_3$ heterostructures" [APL Mater. 4, 016104 (2016)]
APL Materials **5**, 029901 (2017); 10.1063/1.4975656

Fabrication of bit patterned media using templated two-phase growth

Vignesh Sundar,[1,a] XiaoMin Yang,[2] Yang Liu,[3] Zhengkun Dai,[1] Bing Zhou,[3] Jingxi Zhu,[4,5] Kim Lee,[2] Thomas Chang,[2] David Laughlin,[3] and Jian-Gang (Jimmy) Zhu[1]

[1]*Department of Electrical and Computer Engineering, Carnegie Mellon University, Pittsburgh, Pennsylvania 15213, USA*
[2]*Seagate Technology, Fremont, California 94538, USA*
[3]*Department of Materials Science and Engineering, Carnegie Mellon University, Pittsburgh, Pennsylvania 15213, USA*
[4]*Sun Yat-sen University-Carnegie Mellon University Joint Institute of Engineering, Guangzhou, China*
[5]*Sun Yat-sen University-Carnegie Mellon University Shunde International Joint Research Institute, Guangdong, China*

In fabricating high areal density magnetic nanostructures for bit patterned magnetic recording media, conventional lithography methods are limited in scaling and often present other challenges, for instance, as etch-damage in case of subtractive schemes. In this paper, we present a novel two-phase growth scheme that enables the fabrication of nanostructures of one material embedded in a matrix of a different material by choosing a separation material that is immiscible with the material of the nanostructure and by designing a template whose material and morphology guides the separation of the two phases and their subsequent growth. © *2017 Author(s). All article content, except where otherwise noted, is licensed under a Creative Commons Attribution (CC BY) license (http://creativecommons.org/licenses/by/4.0/).* [http://dx.doi.org/10.1063/1.4974866]

When two immiscible species are co-sputtered, the resulting thin film microstructure is affected by both the sputtering conditions and the nature of the substrate surface. Structure-zone diagrams[1] such as the Thornton diagram[2] provide guides for understanding the influence of various parameters on the film microstructure. When the substrate is patterned into having a dome-morphology, as illustrated in Figure 1, and by selecting a substrate material such that the surface mobilities of the immiscible sputtered species on the substrate are different, the sputtered film grows in such a way that the species with the higher surface mobility moves to the trenches between the domes, while the species with the lower mobility is retained on the tops of the domes. This results in a microstructure with spatially isolated nanodots (which can be either single crystalline or polycrystalline) of one material in a matrix of the other material. This can be understood by considering the two different aspects present here. When sputtering is done onto a curved surface, the diffusion of material occurs from the top of the domes, which are regions of positive curvature, to the trenches, which are regions of negative curvature.[3,4] This results in eventual smoothening of the dome-morphology. Additionally, if there are two species with different interface energies being sputtered on the dome-morphology, the species with higher diffusivity therefore will accumulate in the trenches.

The microstructure obtained using such a template growth technique may be a good alternative to the current approaches available for the fabrication of one of the potential next-generation recording technologies, Bit Patterned Media (BPM), where patterned magnetic islands act as individual bits.[5] A similar long-range ordered nanostructure was also reported by Albrecht *et al.*, using the template growth paradigm.[6] The previously explored approaches for BPM fabrication[7] can be classified as

---

[a]Author to whom correspondence should be addressed. Electronic mail: vigneshs@andrew.cmu.edu
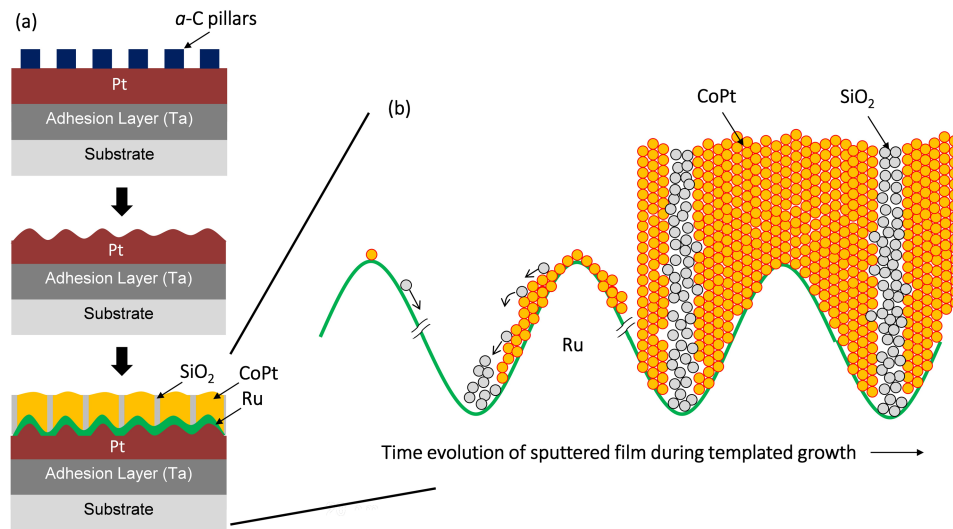
FIG. 1. Evolution of two-phase templated growth during sputtering: (a) schematic of the various steps involved, generating an array of amorphous carbon pillars (a-C), pattern transfer into the Pt template layer using ion-milling, sputtering of Ru and CoPt–SiO$_2$ onto the template. (b) Different species landing on the substrate prepatterned with the dome-morphology experience different mobilities, leading to one species moving to the trench (SiO$_2$) and the other staying on the dome (CoPt). As sputtering continues, this leads to a two-phase microstructure, with regions of CoPt in a matrix of SiO$_2$, the locations of CoPt controlled by the positions of domes in the template.

subtractive or additive. In the case of the subtractive ("top-down") approach,[8,9] the magnetic media film is first deposited as a sheet film and subsequently patterned into pillars using ion-milling or methanol etching, using etch masks defined using e-beam,[10] nanoparticle[11] or nanoimprint lithography, directed block copolymer self-assembly,[12–14] or combinations of these.[15] However, subtractive patterning of magnetic films typically leads to beam damage of the outer pillar surface; a phenomenon that gets exacerbated while scaling to higher bit densities due to the higher damaged surface/undamaged volume of the magnetic pillars. Further, the fabrication of high aspect ratio magnetic pillars using ion milling becomes challenging below 20 nm pitch due to issues such as redeposition and faceting,[16] hence the thickness of the film to be patterned has to be reduced, resulting in lowering of the magnetic volume and therefore the signal. Direct patterning of the magnetic film is avoided by using an additive approach ("bottom-up"), where the substrate is patterned first, and the magnetic media are subsequently deposited.[17] So far, additive approaches have primarily relied on the shadowing effect during sputtering.[18] However, the presence of trench material has been found to result in noise during the recording process. The templated growth technique outlined in this paper can be viewed as a novel additive approach where the two-phase nature of the growth results in the trenches being filled by a non-magnetic segregant.

We demonstrate this concept using the following combination of materials as an example: a cobalt-platinum alloy (CoPt) and silicon oxide (SiO$_2$) as the two immiscible species, and ruthenium (Ru) as the substrate. These materials are exploited in the current perpendicular magnetic recording media, where magnetic CoPt grains with high uniaxial anisotropy are spatially and magnetically isolated by oxide grain boundaries to prevent the magnetizations of adjacent grains from coupling.[19,20] Ruthenium has a hexagonal close packed (HCP) crystal structure with a close lattice matching with HCP CoPt, and thus a coherent Ru–CoPt interface is energetically favored. Further, metal-oxide interfaces are typically higher energy interfaces than metal-metal interfaces.[21–23] This results in higher diffusivity of the oxide species on the metal surface since the diffusivity of the species is proportional to the interface energy.[3] This idea is exploited in current media where the Ru underlayer is sputtered at high pressure, giving rise to dome-shaped Ru grains due to the self-shadowing effect during sputtering, and enabling one-to-one grain matching between the Ru grains and the CoPt grains on top of them along with the better segregation of the oxide to the CoPt boundaries.[24,25] If the domes are artificially patterned into the underlayer, this gives us control over the positions of the CoPt

grains. Rather than patterning the dome-morphology directly into the Ru layer, we used Pt first as the template layer and sputtered a thin layer of Ru subsequently.[26] The process flow is illustrated in Figure 1. The sputtering conditions and tools for the various materials are as follows: Ta (2.5 mT Ar, 4 Å/s), Pt (2.5 mT Ar, 1.3 Å/s), and carbon (5 mT Ar, 0.35 Å/s) were sputtered using DC magnetron sputtering in a 5 target Nanofab sputtering system, while the Ru (5 mT, 0.7 Å/s) and CoPt-SiO$_2$ (45 mT, 1.6 Å/s) films were sputtered using a Z-400 sputtering system fitted with a load lock. The base pressure during sputtering was <2 10^{-7} Torr. Using nanoimprint lithography[10,27] and an oxygen plasma in a *Plasma Therm 790 reactive ion etching system*, a well-ordered hexagonal array of pillars was patterned into a 20 nm amorphous carbon thin film, as observed in the scanning electron micrograph *collected using a FEI Sirion 600 scanning electron microscope* shown in Figure 2(a). The center-to-center spacing between the pillars was 27 nm (1 Tdpsi dot density). The carbon pillars were used as the etch-mask to pattern domes into the Pt template layer. This was done using a Commonwealth Scientfic ion mill. During ion-milling, the substrate was tilted such that the substrate normal was at an angle of 15° with respect to the Ar beam and rotated to ensure uniform milling. Etching and ion-milling conditions are discussed in the supplementary material. The bright field cross section transmission electron micrograph in Figure 2(b) shows the diameter and height of the carbon pillars, which must be optimized along with the ion-milling conditions to obtain the desired morphology in Pt (refer to the supplementary material). Ruthenium and subsequently CoPt–SiO$_2$ were then sputtered onto the template. The resulting film had approximately 11 vol. % of SiO$_2$.

Figure 3(a) shows the plane-view bright field transmission electron micrograph of the final CoPt–SiO$_2$ thin film, observed using a Phillips Tecnai F20 200 FEG transmission electron microscope. The center-to-center distance between the CoPt grains is 27 nm, indicating the "templating" of the media by the Pt domes. The long-range ordering and narrow pitch distribution in the nanoimprint pattern result in a regular final film microstructure with low size distribution. In the high resolution bright field image (Figure 3(b)), we observe the (100) lattice fringes of the crystalline CoPt nanodot, while the brighter region surrounding the nanodot, i.e., the oxide, clearly has an amorphous nature. Lattice fringes are also visible in the adjacent nanodots, with different [100] directions as compared to the central nanodot. Interestingly, the CoPt nanodots in the film have a hexagonal shape. During the ion-milling process, if the mask dimensions and the angle used during milling limit the reach of the ion beam between the pillars, a trace of the deepest trenches will follow the geometry of the pattern, which in this case is hexagonal. Since the oxide fills these trenches and thereby limits the growth of the CoPt, the final microstructure results in the formation of hexagon-shaped nanodots. The indexed electron diffraction pattern (Figure 3(b)) shows the (100) and (110) rings of CoPt and Ru. This, combined with the absence of the (002) diffraction ring shows that the crystallographic texture of the CoPt perpendicular to the plane of the thin films is the desired (002) texture. The observation of the ring pattern indicates the polycrystalline, fiber-textured nature (random crystalline orientations in the plane of the film) of the nanodots, supplementing the observation from the bright field micrographs.
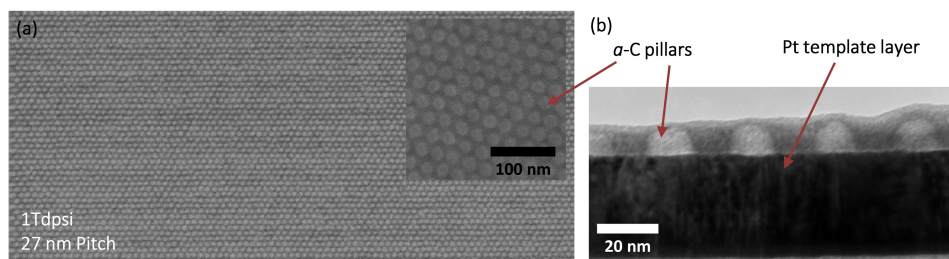

FIG. 2. Mask pillar array determining the positions of domes: (a) plane-view scanning electron micrograph of the long-range ordered 1 Tdpsi amorphous carbon pillar array, inset with a higher magnification. (b) Cross section transmission electron micrograph of the a-C pillars and the Pt template layer; the capping layer on the pillars was added to provide contrast since carbon is light, amorphous, and highly electron transparent.
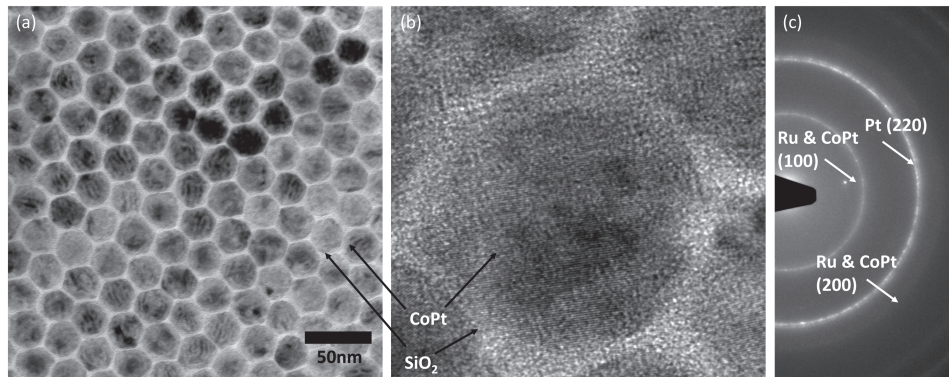
FIG. 3. Plane-view transmission electron microscopy of the templated film: (a) Bright-field micrograph where we observe darker CoPt nanodots surrounded by the brighter SiO_2. (b) High resolution bright field micrograph; the (100) lattice fringes of the CoPt in the central and adjacent CoPt nanodots and the amorphous nature of the oxide can be observed. (c) Plane-view electron diffraction pattern of the templated film indicating the desired (002) crystallographic texture perpendicular to the film plane.

The effect of the template is further illustrated by designing one where only certain regions are fabricated with the dome-morphology. The results are illustrated in Figure 4; while the region patterned with the dome-morphology results in the hexagonal shaped CoPt nanodots as before, the region without the Pt domes results in CoPt with a much smaller grain size (Figure 4(a)). Since the CoPt film is magnetic, a comparison of the magnetic hysteresis loops from templated vs untemplated regions also elucidates the differences in the microstructure. These loops were recorded using an in-house built Kerr measurement system with a spot size of approximately 20 microns. The magnetic easy axis in CoPt is along the (002) axis, and since this film is fiber textured with the c-axis perpendicular to the thin film, an out-of-plane hysteresis loop is an easy axis loop. On comparing the two hysteresis loops (Figure 4(b)), we observe that the templated media sample has a higher coercivity (marked H_c in the figure) of approximately 5 kOe as compared to the untemplated sample (~1.5 kOe). Further, on reaching the nucleation field (H_n in Figure 4(b)), we see that the switching behavior is more gradual for the templated specimen. This is due to the difference in switching mechanisms for the two specimens. In the untemplated film, since the oxide is not well-segregated, the CoPt grains are exchange coupled; the magnetic switching thus occurs by domain wall nucleation and propagation. Since the field required for domain wall propagation is typically lower than that required for nucleation, when H_n is reached and an opposite domain nucleates, the switching is immediate, as indicated by the sharp drop in magnetization. On the other hand, if the grains are exchange decoupled due to the formation of a dense oxide boundary as in the templated microstructure, the switching occurs by Stoner-Wohlfarth rotation. As the grains in the film with the lowest switching field switch, the effective demagnetization field in the film (which aids switching) reduces, thereby requiring a slightly higher field for switching the subsequent grains. This causes the shearing in the hysteresis loop.

The out-of-plane X-ray diffraction patterns comparing the templated and un-templated cases are shown in Figure 4(c). More of the Pt film is milled away in the un-templated case since it is not partially masked by the amorphous carbon pillars, resulting in a relatively low intensity for the Pt (111) peak. The CoPt and Ru (002) peaks, on the other hand, have a higher intensity for the un-templated sample as compared to the templated sample, indicating an inferior texture for the templated case. Another interesting observation in the templated case is that the CoPt (002) peak has shifted closer to the Ru (002) peak. This is possibly due to the deposition of CoPt on the curved Ru surface, resulting in better epitaxy due to the larger and three-dimensional interaction area. The inferior texture in the templated sample is then possibly caused by a similar interaction between the curved Pt dome and the Ru. The difference in stacking between the FCC (111) textured Pt (ABCABC stacking) and the HCP (002) textured Ru (ABABAB) stacking results in the formation of defects at the interface detrimentally affecting the Ru texture. Further research is needed to understand these and other effects of the surface curvature on the texture of the magnetic film, and how it can be improved.
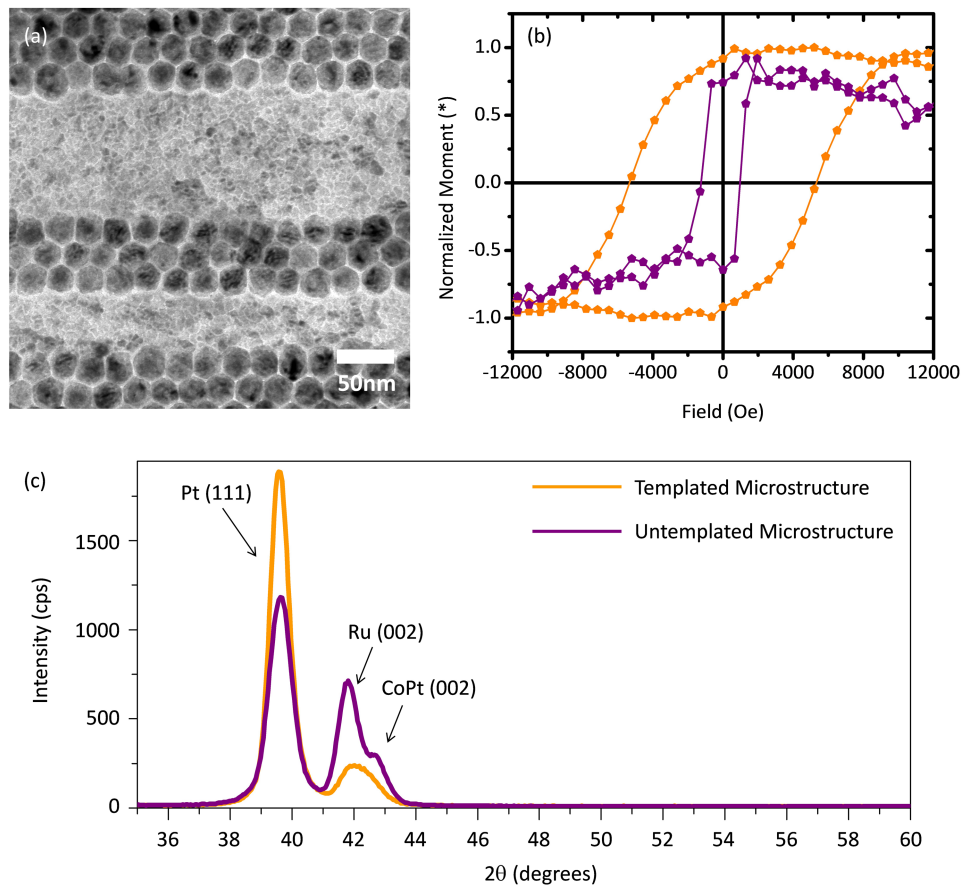
FIG. 4. Comparisons between templated and untemplated films: (a) plane-view transmission electron micrograph with both templated and untemplated regions illustrating the difference in film microstructures. While the templated film has approximately 26 nm grain size and is arranged in a regular fashion as per the template, the untemplated region has a much smaller grain size. (b) Out-of-plane magnetic hysteresis loops collected from templated (orange) and untemplated (purple) regions using the magneto-optic Kerr effect, illustrating the higher coercivity and exchange decoupled nature of the templated film, supporting the conclusions drawn from the microstructure. (c) Out-of-plane x-ray diffraction patterns indicating the desired (002) texture of the Ru and CoPt for both the templated (orange) and untemplated (purple) films, on the (111) textured Pt template layer.

With respect to bit patterned media, the template growth technique has the advantage that it results in fill-factors (magnetic volume fraction) not achievable by subtractive patterning techniques. An additional advantage of the templated growth technique is that it is scalable to sub-20 nm patterns. The patterning requirements in this case, i.e., the fabrication of domes in a suitable material, are less stringent than the direct patterning requirements for magnetic thin films, wherein vertical sidewalls with minimum beam damage has to be achieved. Furthermore, any damage to the surface of the template can be countered by sputtering a thin intermediate film with the suitable texture to generate a pristine crystalline surface prior to the sputtering of the magnetic film, as we did in this case.

The templated two-phase growth technique enables the fabrication of thin films where precise locations can be designed to have different properties. This can be achieved by fabricating templates where only selected regions are patterned with the dome-morphology that enables templated growth, as in Figure 4. While we have showcased the templated growth concept in this letter using a hexagonal array of CoPt nanodots surrounded by SiO_2, the concept can be further applied to generate arrays with different symmetries, and exploring different combinations of materials to realize desired and novel microstructures.

See supplementary material for the development of suitable mask structure for fabricating Pt dome morphology.

[1] B. A. Movchan and A.V. Demchishin, Fiz. Met. Met. (Phys. Met. Met.) **28**, 653 (1969).

[2] J. A. Thornton, Annu. Rev. Mater. Sci. **7**, 239 (1977).

[3] W. W. Mullins, J. Appl. Phys. **30**, 77 (1959).

[4] A. L. Giermann and C. V. Thompson, J. Appl. Phys. **109**, 083520 (2016).

[5] B. D. Terris and T. Thomson, J. Phys. D: Appl. Phys. **38**, R199 (2005).

[6] T. R. Albrecht, H. Arora, V. Ayanoor-vitikkate, J. Beaujour, D. Berman, A. L. Bogdanov, Y. Chapuis, J. Cushen, E. Elizabeth, G. Doerk, H. Gao, M. Grobis, B. Gurney, W. Hanson, T. Hirano, P. Jubert, D. Kercher, J. Lille, Z. Liu, C. Mathew, Y. Obukhov, K. C. Patel, K. Rubin, R. Ruiz, M. Schabes, and L. Wan, IEEE Trans. Magn. **1**, 1 (2015).

[7] B. D. Terris, J. Magn. Magn. Mater. **321**, 512 (2009).

[8] H. Wang, M. T. Rahman, H. Zhao, Y. Isowaki, Y. Kamata, A. Kikitsu, and J.-P. Wang, J. Appl. Phys. **109**, 07B754 (2011).

[9] K. Naito, H. Hieda, M. Sakurai, Y. Kamata, and K. Asakawa, IEEE Trans. Magn. **38**, 1949 (2002).

[10] X. Yang, S. Xiao, W. Wu, Y. Xu, K. Mountfield, R. Rottmayer, K. Lee, D. Kuo, and D. Weller, J. Vac. Sci. Technol., B: Microelectron. Nanometer Struct. **25**, 2202 (2007).

[11] T. Wen, R. A. Booth, and S. A. Majetich, Nano Lett. **12**, 5873 (2012).

[12] R. Ruiz, H. Kang, F. A. Detcheverry, E. Dobisz, D. S. Kercher, T. R. Albrecht, J. J. De Pablo, and P. F. Nealey, Science **321**, 936 (2008).

[13] I. Bita, J. K. W. Yang, Y. S. Jung, C. A. Ross, E. L. Thomas, and K. K. Berggren, Science **321**, 939 (2008).

[14] S. Park, D. H. Lee, J. Xu, B. Kim, S. W. Hong, U. Jeong, T. Xu, and T. P. Russell, Science **323**, 1030 (2009).

[15] T. R. Albrecht, D. Bedau, E. Dobisz, H. Gao, M. Grobis, O. Hellwig, D. Kercher, J. Lille, E. Marinero, K. Patel, R. Ruiz, M. E. Schabes, L. Wan, and D. Weller, IEEE Trans. Magn. **49**, 773 (2013).

[16] M. T. Moneck and J. Zhu, *Dekker Encyclopedia of Nanoscience and Nanotechnology* , 2nd ed. (CRC Press, 2013), pp. 1–23.

[17] O. Hellwig, J. K. Bosworth, E. Dobisz, D. Kercher, T. Hauet, G. Zeltzer, J. D. Risner-Jamtgaard, D. Yaney, and R. Ruiz, Appl. Phys. Lett. **96**, 52511 (2010).

[18] O. Hellwig, A. Moser, E. Dobisz, Z. Z. Bandic, H. Yang, D. S. Kercher, J. D. Risner-Jamtgaard, D. Yaney, and E. E. Fullerton, Appl. Phys. Lett. **93**, 192501 (2008).

[19] S. N. Piramanayagam and K. Srinivasan, J. Magn. Magn. Mater. **321**, 485 (2009).

[20] T. Oikawa, M. Nakamura, H. Uwazumi, T. Shimatsu, H. Muraoka, and Y. Nakamura, IEEE Trans. Magn. **38**, 1976 (2002).

[21] J. S. Chen, J. F. Hu, B. C. Lim, Y. F. Ding, G. M. Chow, and G. Ju, IEEE Trans. Magn. **45**, 839 (2009).

[22] G. Yang, D. L. Li, S. G. Wang, Q. L. Ma, S. H. Liang, H. X. Wei, X. F. Han, T. Hesjedal, R. C. C. Ward, A. Kohn, A. Elkayam, N. Tal, and X.-G. Zhang, J. Appl. Phys. **117**, 083904 (2016).

[23] B. Drevet and N. Eustathopoulos, Metall. Mater. Trans. A **25**, 599 (1994).

[24] J. Z. Shi, S. N. Piramanayagam, C. S. Mah, H. B. Zhao, J. M. Zhao, Y. S. Kay, and C. K. Pock, Appl. Phys. Lett. **87**, 222503 (2005).

[25] S. H. Park, S. O. Kim, T. D. Lee, H. S. Oh, Y. S. Kim, N. Y. Park, and D. H. Hong, J. Appl. Phys. **99**, 08E701 (2006).

[26] V. Sundar, J. Zhu, D. E. Laughlin, and J.-G. J. Zhu, Nano Lett. **14**, 1609 (2014).

[27] X. Yang, Y. Xu, C. Seiler, L. Wan, and S. Xiao, J. Vac. Sci. Technol., B: Microelectron. Nanometer Struct. **26**, 2604 (2008).